The Journal of Chemical Physics

AIP Publishing

Ultrafast X-ray Scattering of Photodissociation Dynamics in 2-Iodothiophene

Weronika O. Razmus,[†] Ian Gabalski,[‡] Felix Allum,[‡] Grite L. Abma,[§] Mathew Britton,[‖] Sébastien Boutet,[‖] Philip H. Bucksbaum,[‡] Xinxin Cheng,[‖] Stuart W. Crane,[⊥] Gregory Gate,[‖] Aaron Ghrist,[‡] Martin Graßl,[‡] Alice E. Green,[‡] Nathan Goff,[⊥] Daniel A. Horke,[§] Lisa Huang,[⊥] Mengning Liang,[‖] Yusong Liu,[‖] Lingyu Ma,[⊥] Michael P Minitti,[‖] Thomas Northey,[⊥] Asami Odate,[⊥] Joseph Robinson,[‖] Peter M. Weber,[⊥] Thomas Wolf,[‖] Basile F. E. Curchod,[△] Michael N. R. Ashfold,[△] Russell Minns,[*,†] and Ruaridh Forbes[*,‖,∇]

†*School of Chemistry and Chemical Engineering, University of Southampton, Highfield, Southampton, SO17 1BJ, UK*

‡*PULSE Institute, SLAC National Accelerator Laboratory, 2575 Sand Hill Road, Menlo Park, CA 94025, USA*

¶*Center for Free-Electron Laser Science CFEL, Deutsches Elektronen-Synchrotron DESY, Notkestr. 85, 22607 Hamburg, Germany*

§*Institute for Molecules and Materials, Radboud University, Heijendaalseweg 135, 6525 AJ Nijmegen, The Netherlands.*

‖*Linac Coherent Light Source, SLAC National Accelerator Laboratory, 2575 Sand Hill Road, Menlo Park, CA 94025, USA*

⊥*Department of Chemistry, Brown University, Providence, Rhode Island 02912, USA*

#*EaStCHEM School of Chemistry, University of Edinburgh, Edinburgh EH9 3FJ, UK*

@*European XFEL, Holzkoppel 4, 22869 Schenefeld, Germany*

△*School of Chemistry, University of Bristol, Cantock's Close, Bristol BS8 1TS, UK*

∇*Department of Chemistry, University of California, Davis, One Shields Avenue, Davis, CA 95616, USA*

E-mail: r.s.minns@soton.ac.uk; ruforbes@ucdavis.edu

The Journal of Chemical Physics

AIP Publishing

Abstract

A time-resolved X-ray scattering (TRXS) investigation of the photodissociation dynamics of gas-phase 2-iodothiophene (2IT) molecules following 252 nm excitation is presented. Structural evolution of the molecule and dynamical information on the resulting photofragments were captured using femtosecond X-ray free-electron laser pulses. Two dissociation pathways were identified, arising via excitation to $\pi\pi^*$ and $(n/\pi)\sigma^*$ states respectively, yielding distinct interfragment recoil velocities of approximately 6.4 Å ps^{-1} and 17.0 Å ps^{-1}. Comparison of asymptotic scattering data with simulated patternsindicates that the thiophene ring remains closed following dissociation at this wavelength.Modeling the experimental data yields a branching ratio of ∼3:1 in favor of the high velocity channel. These findings demonstrate the capability of TRXS to disentangle concurrent ultrafast reaction pathways and provide detailed structural insight into energy redistribution during photoinduced bond fission in complex molecular systems.

Introduction

Ultrafast X-ray scattering has emerged as a transformative technique for directly observing molecular structural dynamics during photochemical reactions.[1–14] By combining the atomic-scale spatial resolution of X-ray scattering with femtosecond temporal resolution provided by X-ray free-electron lasers, this approach enables real-time visualization of bond breaking, formation, and rearrangement processes that govern chemical reactivity. Unlike traditional spectroscopic methods that provide indirect structural information, time-resolved X-ray scattering directly probes internuclear distances as they evolve, offering insight into the fundamental mechanisms of photochemistry.

A landmark demonstration in the field of time-resolved X-ray scattering (TRXS) of gas-phase molecules was demonstrated by Minitti *et al.* in their 2015 study of 1,3-cyclohexadiene (CHD) photoisomerisation .[4] This work directly imaged the ring-opening reaction following

267 nm excitation using 8.3 keV, 30 fs X-ray pulses, capturing the structural transformation with an 80 fs time constant that closely matched the 140 fs electronic state decay observed spectroscopically. By comparing experimental scattering patterns with advanced trajectory calculations using 100 different starting conditions, this study definitively established that X-ray scattering could visualize concerted structural rearrangements in gas-phase complex organic molecules with atomic-scale resolution and femtosecond temporal resolution.

The capabilities have since been systematically extended to increasingly sophisticated molecular targets, revealing new insights into ultrafast reaction dynamics.[5–9,11] The challenge of molecules far from thermal equilibrium has been systematically addressed through molecular dynamics-based analysis approaches. Studies of vibrationally hot CHD (effective temperature ∼2870 K, 6.2 eV internal energy)[6] demonstrated that transition state structures make significant contributions to scattering signals, requiring molecular dynamics simulations with over 200,000 structures to properly account for anharmonicity and correlated motions that cannot be captured by harmonic approximations.[6] Recent work on 1,2-dithiane photodissociation revealed multiple competing fragmentation pathways with time constants of 240 fs, 1.05 ps, and 63 ps, ultimately yielding product branching ratios of 35% and 65% for different dissociation channels, demonstrating the technique's ability to quantitatively characterize complex reaction networks.[11]

Complementing these time-domain measurements, frequency-resolved X-ray scattering (FRXS) has emerged as a powerful analysis tool for disentangling complex dynamics when multiple overlapping processes occur simultaneously. Building on the foundational molecular work, Bucksbaum,[12] Gabalski,[1] and Ware[3,13,15] developed FRXS analysis methods using molecular iodine following 800 nm multiphoton excitation, demonstrating how this approach could separate overlapping dissociation channels with interfragment terminal velocities of 23 Å ps^{-1} and 14 Å ps^{-1} while extracting an early-time acceleration timescale of 11 fs that quantified the duration of repulsive forces during bond breaking. Further work on FRXS analysis of CS_2 photodissociation at 200 nm[2] revealed coherent bending vibrations within the

first 150 fs, while clearly separating singlet and triplet dissociation channels that evolved from mixed velocity distributions (24 Å ps^{-1}) at early times to predominantly triplet character (28 Å ps^{-1}) after 1400 fs. FRXS therefore offers a complementary perspective to time-domain TRXS data by Fourier-transforming the scattering signal along the time-axis.[1,2,12,15] This transformation decomposes the signal into its constituent frequency components, providing a sparser representation that can reveal underlying periodicity or trends. When plotting signal as a function of frequency, ω, and momentum transfer, Q, coherent vibrational motion appears as sharp peaks at characteristic vibrational frequencies, while dissociative motion manifests as slanted lines. As such, FRXS enables vibrational and dissociative dynamics to be cleanly separated and analyzed, providing critical mechanistic information without requiring full knowledge of the potential energy surfaces.

Molecules such as 2-iodothiophene (2IT) provide opportunities to test these approaches as they occupy a unique middle ground: they are sufficiently complex to exhibit multiple excited state pathways and rich energy redistribution over multiple modes, yet remain accessible for detailed experimental investigations. With multiple accessible electronic states and a flexible molecular framework, 2IT exhibits richer dynamics than simple systems, including competing dissociation pathways and internal energy redistribution. Furthermore, 2IT possesses two chromophores in the C-I bond and the aromatic thiophene ring. Building on established capabilities for studying heterocyclic ring dynamics, competing dissociation channels, and electronic structure effects, 2IT represents an ideal platform for investigating how molecular complexity shapes ultrafast reaction dynamics while testing the limits of current FRXS analysis methods for disentangling multi-pathway photochemistry in substituted heterocycles.

The UV induced photodissociation dynamics of 2IT are governed by a complex interplay between the excitation of different electronic states and subsequent redistribution of energy among the nuclear degrees of freedom. Studies of bare thiophene and thiophenone, where UV absorption predominately populates a $\pi\pi^*$ state leading to C–S bond extension, ring

puckering, and relaxation to the ground-state, reveal ring-opening as one potential decay pathway.[16–22] The addition of an iodine atom introduces new reaction channels. In 2IT, photoexcitation can populate either the $\pi\pi^*$ states associated with the thiophene ring or the $(n/\pi)\sigma^*$ states involving a C-I bond localized σ^* orbital, which facilitate efficient C-I bond fission.[23,24] Resonance Raman measurements, performed on 2IT in cyclohexane at 245.9 nm and 252.7 nm, have provided evidence for the simultaneous activation of C–I bond stretching and skeletal vibrational modes of the ring, suggesting the possibility of relaxation through C-I or C-S bond extension.[25] More recent ultrafast extreme ultraviolet spectroscopy (XUV) transient absorption measurements around the I 4d edge, following 268 nm photoexcitation,[24] have shown that the dominant process at this wavelength is rapid dissociation of the C-I bond and iodine atom formation on a 160 ± 30 fs timescale. Within this measurement Toulson *et al.* also obtained a I to I* branching ratio of 0.77 to 0.23 suggesting that formation of the ground spin-orbit state is the dominant channel.[24]

More detailed information has been obtained through ion imaging experiments that measure the velocities of the iodine atoms formed following UV absorption. Nanosecond Resonance-Enhanced Multiphoton Ionization (REMPI) detection of the ground (I) and spin-orbit excited (I*) atom products were performed at several wavelengths in the range ∼278-220 nm.[23] The total kinetic energy release (TKER) distributions in all cases showed two components. One yields fast I/I* fragments with anisotropic angular distributions, consistent with prompt C-I bond fission. The second produced slower I/I* atom products, with isotropic recoil velocity distributions. These were suggested to originate from molecules that undergo nonadiabatic relaxation to highly vibrationally excited ground state species prior to C-I bond fission. The ratio of the slow to fast component was seen to increase as the pump wavelength decreased. More recent femtosecond resolved measurements performed at a pump wavelength of 262 nm detected similar distributions following X-ray ionization of iodine atoms.[26] These experiments are insensitive to the spin-orbit state of the iodine atom. But, in common with the nanosecond experiments, the femtosecond experiments identified a

direct dissociation channel yielding iodine atoms with strong parallel recoil anisotropy, and slower products with isotropic velocities. The iodine atoms arising via this latter channel appeared after a delay of 1 ps. These observations led to the conclusion that the two pathways arise from initial excitation into a superposition of $(n/\pi)\sigma^*$ and $\pi\pi^*$ states, with the $\pi\pi^*$ states being bound along the C-I coordinate, causing transient trapping of the excited state population. This was supported by a measurement of ultraviolet absorption cross-sections which suggested non-negligible excitation into both states at the employed wavelength. The 'fast' to 'slow' branching ratio at 262 nm was determined to be approximately 23:1 in favor of the direct vs the indirect dissociation channel,[26] which is broadly consistent with expectations based on the measured relative absorption cross-sections of the involved states.[26] Furthermore, in both experiments the indirect dissociation products were found to be released with kinetic energies much lower than the maximum allowed by energy conservation rules, implying a significant partitioning of excess energy into internal degrees of freedom, particularly rotational and vibrational excitation of the thiophenyl co-fragment.[23,26] Neither the REMPI or site-selective X-ray ionization studies returned I/I* branching ratios. Furthermore, the focus on the iodine fragment produced means that none of the experiments have been able to directly measure the characteristics of the co-fragment and confirm wether it remains as a cyclic species or if ring-opening plays a significant role.

In the present work, the structural dynamics of 2IT photodissociation were explored using ultrafast TRXS following excitation at 252 nm, a shorter wavelength than in our previous work.[26] Based on our previous conclusions, the increase in photoexcitation energy is expected to increase the partial cross-section for excitation into the $\pi\pi^*$ state, thus increasing the contribution of the indirect dissociation pathway. By employing TRXS and FRXS analyses, we directly characterize the structural evolution of photoexcited 2IT, quantifying the interfragment dissociation velocities, branching ratios, and the nature of the co-fragment ring structure. Furthermore, by modeling the scattering data using simple dynamical models, including bond extension and rotational excitation, we assess the partitioning of energy

during photodissociation. Through this approach, we provide new structural insights into the photo-induced dissociation of the iodinated heterocycle.

Experimental Details

X-ray scattering data from UV-excited 2IT molecules were collected at the CXI instrument of the LCLS.[27] The gas-phase sample was introduced into a continuous gas flow cell equipped with a beryllium out-coupling window to minimize the absorption and re-scattering of scattered X-rays.[8] The sample was photoexcited by a 252 nm, 1.6 μJ laser pulse with a duration of 50 fs full-width at half maximum (FWHM), derived from an optical parametric amplifier pumped by a Ti:Sapphire amplifier. After a controlled time delay, the sample was probed using 15 keV X-ray pulses generated by the LCLS.

Scattered X-rays were detected using a Jungfrau hard X-ray pixel detector, with a pixel size of 75 μm, and operated in variable-gain mode.[28] The detector was positioned approximately 8 cm downstream from the scattering cell. Raw detector images were first thresholded to eliminate electronic noise. X-ray hits were then identified and localized within 2×2 pixel regions. Only hits with energy values consistent with an integer number of coherently scattered photons were retained for further analysis, this is to exclude any fluorescence signal. Subsequent corrections were applied to account for the variation in the Thomson scattering cross-section with respect to the X-ray polarization direction.[8] The detector geometry was precisely calibrated by fitting the static scattering pattern of sulfur hexafluoride (SF_6) to its known elastic and inelastic scattering profiles.[8]

Pump-probe measurements were recorded by systematically varying the delay between the UV pump laser and X-ray pulses. Individual shots were time-binned using a cross-correlation monitor ("time-tool") to correct for shot-to-shot timing jitter between pump and probe pulses.[29] The time-tool enabled arrival-time corrections with a resolution of better than 10 fs.[29] Approximately 18% of the shots were recorded with the pump laser delayed by

several nanoseconds to obtain the background (unpumped) scattering signals for subtraction.

Individual shots were excluded from the analysis if the X-ray pulse energy was more than one standard deviation outside of the mean, or if the time-tool jitter correction fit failed. Overall, approximately 30% of the pump-probe shots were rejected based on these criteria.

The time-resolved scattering signal was obtained by azimuthally integrating the individual detector images and sorting them into 25 fs time bins in the range -500 to 2000 fs, where negative times correspond to the X-ray probe pulse preceding the UV photoexcitation pulse. The time-resolved difference signal used in the analysis presented below was obtained by subtracting the unpumped (background) scattering signal from the scattering signal in each of the time bins:

$$\Delta I(Q,t) = 100\% \times \frac{I(Q,t) - I_{\text{off}}(Q)}{I_{\text{off}}(Q)} \tag{1}$$

where t is the pump-probe delay, and Q is the momentum transfer.

The time-zero (pump-probe temporal overlap) was determined by fitting a logistic function to the rising edge of the pump-probe signal. Statistical uncertainty was assessed using bootstrapping.

Results and Discussion

Time-resolved X-ray Scattering

The changes in the measured scattering pattern in percent as a function of the pump-probe delay, t and the momentum transfer, Q, are shown in Figure 1. Immediately following 252 nm excitation (i.e. after time-zero), the difference scattering signal manifests as an oscillating pattern along the momentum transfer Q. The intensity enhancements and depletions relative to ground-state scattering are represented in red and blue, respectively. In contrast to most spectroscopic methods, these features are interdependent and do not individually correspond

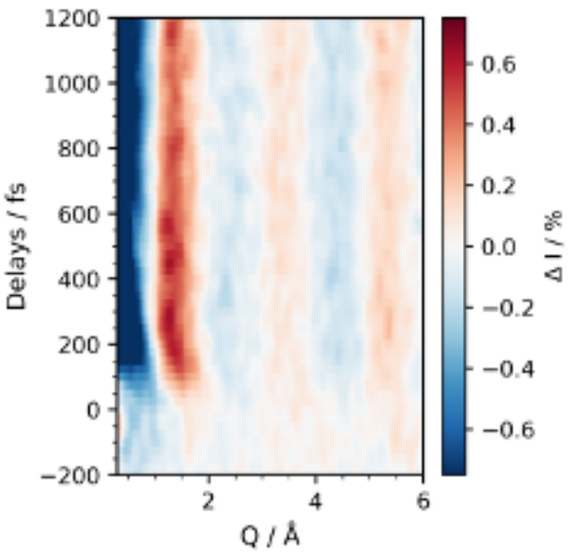

Figure 1: Time-resolved, azimuthally averaged, difference X-ray scattering signal following photoexcitation of 2IT at 252 nm.

to the populations of distinct states. Each internuclear distance within 2IT contributes a sinusoidal component to the total measured scattering pattern. Consequently, changes in any of these distances relative to the ground-state 2IT are projected as changes in the amplitude as well as positions of the maxima and minima of the difference pattern.

Nonetheless, the features of the observed difference scattering pattern are consistent with the increasing interatomic separation. First, the feature observed at the lowest Q values in Figure 1 is a depletion indicating overall reduction in scattering intensity as a result of molecular fragmentation.[14,30] This arises from the fundamental nature of coherent X-ray scattering from molecular systems. At $Q = 0$, the total scattering signal is proportional to the square of the number of electrons in the scattering volume.[14] For an intact molecule with N electrons, the signal scales as N^2. Upon fragmentation into two pieces with F_1 and F_2 electrons, respectively (where $F_1 + F_2 = N$), the scattering signal becomes proportional to $F_1^2 + F_2^2$. Since $F_1^2 + F_2^2$ is less than $(F_1 + F_2)^2$, fragmentation always results in reduction of scattering intensity at low Q. Physically this is due to the loss of coherent scattering between electrons that are now separated into different fragments.[14]

Additionally, there is a notable shift in the peak positions toward lower Q values over the course of the first 300 fs. This shift is indicative of increasing bond lengths as is expected in dissociation. This shift can be understood by considering the rotationally averaged Independent Atom Model (IAM):[30]

$$I_{\mathrm{IAM}}(Q) = \sum_{i,j}^{N_{\mathrm{at}}} f_i(Q) f_j(Q) \frac{\sin Q r_{ij}}{Q r_{ij}} + \sum_{i}^{N_{\mathrm{at}}} I_{\mathrm{inel},i}^{\mathrm{IAM}}(Q) \tag{2}$$

where $f_i(Q)$ is the scattering form factor of the ith atom, the i and j are the atoms present in the molecule and r_{ij} is the distance between atoms i and j. Inelastic contributions to the overall scattering signal (known as Compton Scattering) are given by the term $I_{\mathrm{inel},i}^{\mathrm{IAM}}(Q)$. The term $\frac{\sin Qr}{Qr}$ describes how pairs of atoms contribute to the scattering pattern. Each pair of atoms separated by distance r_{ij} contributes a Bessel function that approaches unity as $\mathrm{Q} \to 0$. As r_{ij} increases during bond dissociation, the oscillation frequency of the Bessel function increases, but the main features in the pattern (maxima and minima) shift toward lower Q values because the first maximum of $\frac{\sin Qr}{Qr}$ occurs at $Q = \pi / r_{ij}$. This means that longer interatomic distances result in peak positions shifting to smaller Q values.

These observations provide preliminary evidence for the presence of dissociation dynamics. However, the one-dimensional projection inherent to scattering measurements is limited in terms of disentangling significant concurrent structural changes. In particular, overlapping contributions from multiple evolving bond lengths can obscure mechanistic interpretations when used solely in the momentum transfer domain. This is significant here, as previous studies, performed on 2IT at similar wavelengths, show that the C-I bond length evolves concurrently on two distinct time scales, which is hard to distinguish in the current representation of the data.[26] To facilitate further interpretation of the TRXS results, FRXS was employed.[1–3,12,15]

Frequency-resolved X-ray Scattering

FRXS is a method to analyze TRXS data by separating the different frequency components present in the scattering pattern, thus offering a sparser representation of the data.[1–3,12,13,15] This facilitates the identification of the underlying nuclear dynamics. The FRXS power spectrum is generated by Fourier transforming the time-dependent scattering signal at each value of momentum transfer Q. In this representation of the data, distinct dynamical processes give rise to characteristic features. Vibrational motions, which are periodic and localized around the equilibrium geometries, appear as horizontal bands of intensity. These bands are centered on the vibrational frequency, with their extent in the Q-space reflecting the spatial scale of the bond displacement associated with each vibrational mode.[12,15]

In contrast, bond dissociation processes, which are inherently non-periodic and directional, manifest as slanted lines in the FRXS spectrum. As the atoms move apart during dissociation, their increasing separation gives rise to time-dependent modulation of the scattering signal with a continuously varying phase. This motion projects onto the FRXS spectrum as slanted features in Q-ω space with maxima along the line defined by $\omega = Qv$, where v is the interfragment separation velocity of the fragments.[15] Characterizing these lines provides a direct means of extracting the separation velocity of the fragments formed in the dissociation process from the experimental data.

In previous work on molecular I_2, these high-intensity features in the FRXS spectrum have been visually identified.[3,12,13,15] In studies of small molecules, this approach proved effective because the vibrational and dissociative features were typically sharp and well separated within the Q-ω space. The limited number of single parent vibrational mode, lack of internal degrees of freedom in the dissociation products, and the relatively simple dissociation pathways allowed for a clear interpretation without the need for advanced data analysis techniques. However, as the size and complexity of the target molecule increases, this approach has become increasingly impractical.[2,15] Larger molecules, such as 2IT, possess many vibrational degrees of freedom (21), and denser manifolds of vibrational states that can be

populated upon excitation and/or through the dissociation process itself. Additionally, their dissociation can produce rotating co-fragments, further broadening the features in FRXS spectra as the available energy is partitioned among dissociative and rovibrational modes. This increased complexity leads to significant overlap between spectral features, resulting in an FRXS pattern that is not amenable to manual interpretation. The FRXS spectrum of 2IT, shown in Figure 2c, illustrates this point clearly: no distinct features can be readily identified by eye. For an example FRXS analysis of a simple dissociation reaction, we refer the reader to Figure 3 of Ware et al.[3] that shows experimental and theoretical plots for the photolysis of I_2. Clear diagonal features appear in the FRXS spectrum due to the narrow distribution of interfragment velocities produced upon bond breaking. To overcome these limitations, mathematical feature extraction methods have recently been employed.[1,2,12] In the current study, a Hough transform based approach was adopted from Ref.[2]

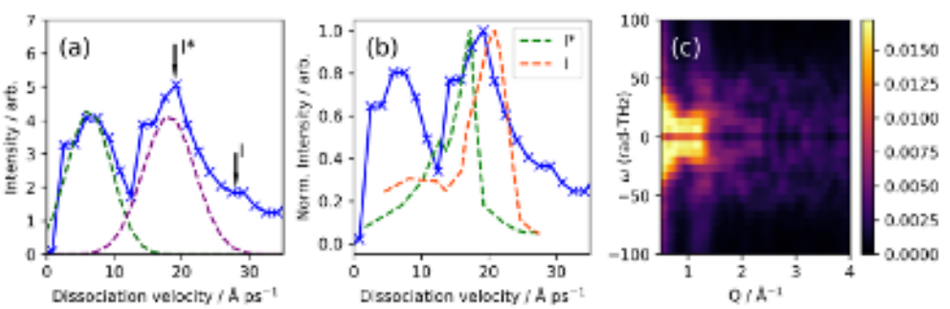

Figure 2: a) Velocity-resolved Hough intensity along the $v_0 = 0$ coordinate following applying the Hough transform to experimental FRXS spectrum in the range 0-1.1 ps and Q = 0.75-4 Å^{-1}, shown in blue with 'x' marking the data points. Components of a two Gaussian fit (described in text) are shown as dashed lines representing the interfragment velocity distributions of the "fast" (purple) and "slow" (green) pathways. Black arrows mark the maximum allowed dissociation velocity based on conservation of energy for channels yielding I and I* atoms. b) Velocity-resolved Hough intensity from panel a) alongside the REMPI distributions for the I (red) and I* (green) atomic fragments at a photoexcitation wavelength of 254.7 nm.[23] We note that each distribution is normalized to the same maximum intensity and therefore does not reflect the branching ratio between the two product channels. c) The experimental FRXS spectrum produced by Fourier transforming the measured difference scattering pattern in the range 0-1.1 ps and Q = 0.75-4 Å^{-1}

Hough Transform

The Hough transform analysis provides a more robust means of identifying linear features within the FRXS power spectrum, allowing systematic detection and characterization of dissociation signatures in systems where manual identification is unreliable. An additional advantage of employing the Hough transform approach is its ability to extract a distribution of dissociation velocities rather than a singular value, offering a more nuanced view of the dissociation process.

The Hough transform is a mathematical operation that maps lines present in an input image (here the FRXS spectrum) into single points in a transformed representation. In the FRXS data, the slanted bands of intensity associated with primary dissociations originate near $v_0 = 0$, corresponding to fragments that accelerate from an initially bound geometry. To extract these features, the Hough transform is used to systematically analyze the FRXS spectrum by mapping each point in the FRXS space to a curve in Hough space. This is because each point can lie on a family of lines with different slopes and intercepts.[2,12] If a linear feature, such as a dissociation trajectory, is present in FRXS space, the corresponding curves from all points along that feature will intersect at a single point in Hough space, revealing its presence and parameters. In this study, the transform was applied to identify features corresponding to interfragment separation velocities up to 40 Å ps^{-1}.

To prepare the data, the TRXS spectrum was Fourier transformed in the range of 0-1 ps in the Q region 0.75-4 $\mathring{A}^{-1}$, producing the FRXS spectrum for analysis. The Hough transform was then applied to this spectrum as outlined above. The chosen time window provides a sufficiently large time domain to identify the pathways resulting in dissociation velocities up to the maximum possible value based on the difference between the photon energy and C-I bond energy. Meanwhile, restricting the Q-range improves the accuracy of the subsequent Hough transform by excluding the region of the data where the noise level becomes large enough to introduce artifacts. A lineout from the two-dimensional Hough transform is shown in Figure 2, as a function of the relative dissociation velocity. The lineout is taken along

the $v_0 = 0$ axis. This specific slice was chosen because, as mentioned earlier, all primary dissociation features must intersect this point.

The results of the Hough transform show two maxima with broad overlapping distributions. To quantitatively describe the observed velocity distributions, a sum of two Gaussian functions was fitted to the Hough-transformed data. This fitting yielded individual components with mean interfragment separation velocities of 6.4 Å ps^{-1} and 17.0 Å ps^{-1}, and corresponding standard deviations of 3.6 Å ps^{-1} and 3.8 Å ps^{-1}, respectively. The relatively broad widths of these distributions is likely a result of the spin-orbit splitting within the iodine atoms that contribute to each peak in the spectrum and the internal energy spread within the radical co-fragment. Overall, these results are broadly consistent with both site-selective ionization and REMPI studies, which concluded that the C–I bond in 2IT dissociates via two distinct pathways (one direct, the other following non-adiabatic coupling from the initially populated $\pi\pi^*$ state), each of which releases iodine atoms in both spin-orbit states with characteristic interfragment separation velocities centered around 8 and 18 Å ps^{-1}.[23,26] While a direct comparison of absolute velocity values is not appropriate due to differences in excitation wavelengths, there is a clear qualitative agreement.

Although the Hough transform approach provides a powerful tool for FRXS feature extraction, the results must be interpreted with caution, because of several inherent limitations. This method yields the most reliable results when analyzing bands with narrow, separated, and well-defined velocity distributions. In cases where broad or overlapping features are present in the FRXS spectrum, the Hough transform is prone to overestimating the width of the velocity distribution associated with each feature,[15] introducing potential bias to further interpretations of the dynamics at play. The visibility of features in the Hough representation is further reduced when applied to systems where dissociation occurs over a distribution of times.[12,15]

Our previous studies on 2IT hypothesized that a predissociation pathway is responsible for the iodine atom products released with low velocities.[26] The presence of a predissociation

step introduces a time delay between photoexcitation and the onset of dissociation, which manifests as a phase shift in the FRXS data. The phase shift caused by a time delay τ, is given by $e^{i\omega\tau}$. When dissociation occurs over a range of time delays, the corresponding signal in the FRXS power spectrum is effectively averaged over multiple phases, leading to a reduction in the overall visibility and sharpness of the dissociation feature.[12,15]

An important note for quantitative analysis is that due to the phase averaging the intensity of a given feature in the Hough-transformed space does not directly reflect the absolute yield of the associated dissociation pathway.[12] As a result, while the Hough transform can successfully identify the presence and approximate velocity distribution of dissociation products, caution must be exercised when calculating values of the reaction yields or branching ratios.

Despite these limitations, the use of the Hough transform is justified in the case of 2IT due to the highly congested nature of its FRXS spectrum and the lack of detailed trajectory simulations, which are typically required for full interpretation of time-resolved scattering data.[1,2,12,15] As discussed above, the dense vibrational manifold and potential rotational excitation of the molecular co-fragment leads to substantial overlap and broadening of features, rendering manual identification infeasible. The Hough method offers an objective means of highlighting dominant dissociative trends, particularly those corresponding to linear trajectories in momentum space, which are otherwise obscured in the raw FRXS data. While it does not capture all the nuances of the dissociation dynamics, especially those affected by phase averaging or overlapping velocity distributions, it provides a tractable approach to isolate and characterize primary velocity components. The information obtained through this approach forms an essential foundation for the further analysis presented in this manuscript.

Asymptotic data analysis

Previous studies of the photodissociation dynamics in 2IT primarily focused on detecting the iodine atom fragment,[23,24,26] while the fate of the co-fragment remained largely inaccessible.

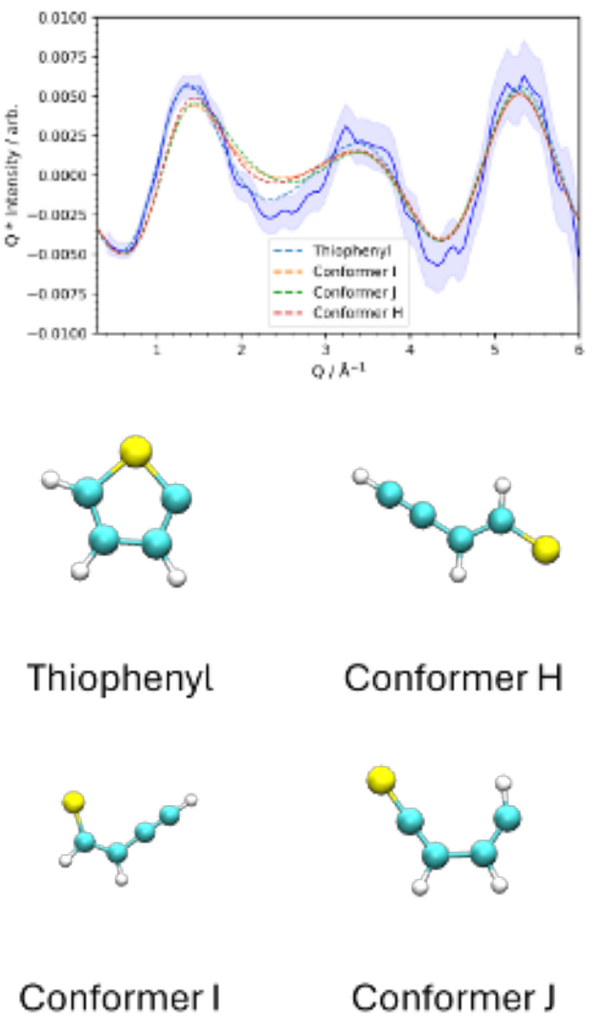

Figure 3: Experimentally measured difference scattering pattern (blue solid line, integrated for pump-probe delays between 1-2 ps with 1 standard deviation marked by the shaded region) overlaid with calculated scattering patterns for plausible co-fragment structures (dashed lines) assuming an infinitely large separation to the atomic iodine co-fragment. Co-fragment structures are shown below the graph.

Techniques such as REMPI[23] and inner-shell ionization[26] are inherently selective for the iodine atom, limiting information about the co-fragment to indirect inference. Although computational calculations suggest the possibility of various final structures for the C_4SH_3 co-fragment,[23] TRXS offers a direct structural probe that can simultaneously capture the geometries of both fragments, providing insight into the co-fragment's structure following C–I bond cleavage.

To characterize the co-fragment structure, we compared the asymptotic experimental scattering pattern with a simulated pattern for the closed-ring thiophenyl radical structure as well as for three other acyclic structures of comparable energy[23] as depicted in Figure 3.The relative energies of fragments H, I and J compared to the thiophenyl radical (0.0 eV) are 0.52 eV, 0.57 eV, and 1.62 eV, respectively. The experimental asymptotic pattern was obtained by averaging scattering data at pump-probe delays between 1-2 ps, when bond cleavage is complete and the system has reached a stable geometry.[24,26] The simulated pattern was generated using the IAM applied to the geometry of the four radical structures optimized using unrestricted density functional theory with the ωB97X-D4 exchange-correlation functional[31,32] and the def2-TZVP basis,[33] as implemented in Orca version 6.0.1.[34]

Figure 3 shows this comparison, with the experimental asymptotic difference scattering pattern as a solid blue line and the simulated patterns associated with the various radical fragments as dashed lines. All patterns were multiplied by Q to enhance visibility, particularly at higher Q values, and the excitation fraction was scaled to optimize the match with experimental data. Despite the inherent simplification, where experimental data represents an average over multiple geometries of the vibrationally hot radical while the simulation corresponds to a single minimum energy structure, the agreement between experiment and the predicted scattering pattern of the ring closed thiophenyl radical is good across the entire measured Q range and much better than that with the acyclic variants of the C_4SH_3 radical in the region between 2-3 $Å^{-1}$.

This correspondence provides evidence that the thiophenyl ring remains structurally in-

tact following C–I bond dissociation. This suggests that the cyclic framework does not undergo significant skeletal rearrangement or ring-opening processes on the experimental timescale, confirming the formation of a stable closed-ring thiophenyl radical as the primary co-fragment following 252 nm excitation of 2IT. The observed 'fast' and 'slow' channels are signatures of, respectively, direct C-I bond fission following excitation to states with dominant nσ^* character, and delayed C-I bond fission from predissociating 2-IT molecules that are initially excited to a $\pi\pi^*$ state with, in both cases, retention of the cyclic thiophenyl radical geometry. The present analysis provides no evidence for any dissociation driven by nonadiabatic coupling to the S_0 state driven by an initial C-S bond extension (ring-opening) - as is found in the UV photolysis of thiophenone[22,35] - and subsequent dissociation to ring-opened products on the S_0 potential energy surface. Note, however, that the present study cannot eliminate the possibility that some vibrationally hot thiophenyl radicals might isomerize to acyclic geometries on much longer timescales.

Data fitting

Building on the conclusion that the thiophenyl ring remains intact following C-I bond cleavage at 252 nm, a simple dynamical model was constructed to further interpret the evolving scattering patterns. In this model, dissociation was implemented by a progressive extension of the C-I bond, while maintaining the geometry of the thiophenyl co-fragment fixed in the closed-ring structure of the dissociated fragment. Later iterations of the model allow for a possible time off-set between the start of the two dissociation channels, and for possible partitioning of internal (e.g. rotational) excitation into the co-fragment. These additions were guided by findings of previous works.[26]

The rate at which the bond extends is extracted from the results of the Hough transform analysis. Each of the two Gaussian components fitted to the overall interfragment velocity distribution was assumed to represent an individual dissociation channel, hereafter referred to as the "slow" and "fast" channels.

For each channel, a normalized simulated spectrum was generated. To construct these spectra, the corresponding Gaussian velocity distribution was sampled at intervals of 0.1 Å ps^{-1}. For each sampled dissociation velocity, the extension of the C–I bond as a function of the pump-probe delay was calculated as $R(t) = R_0 + vt$, where $R(t)$ is the internuclear distance at pump-probe delay t, and R_0 is the C-I equilibrium bond distance (2.05 Å). The evolving bond distance was calculated under the assumption of constant radial velocity and axial recoil. Once the geometry was known, a time-dependent difference scattering pattern was generated by calculating the expected scattering signal, using IAM, at pump-probe delays matching those of the experimental dataset.

A weighted mean of the calculated difference spectra was obtained, where the weights for each sampled velocity were determined by the corresponding intensity of the normalized Gaussian distribution shown in Figure 2. This yielded channel-specific difference spectra that reflected the expected scattering signal based on the experimentally observed distribution of the interfragment dissociation velocities. These channel-specific simulated spectra formed the basis for fitting the experimental scattering data.

The experimental time-resolved scattering spectrum was assumed to be represented by the weighted sum of the fast and slow dissociation channels. The relative contributions of each channel were determined using a least-squares fitting procedure between the experimental data and the simulated scattering patterns described above. The weights of the simulated patterns were set as the free parameters in the fit and yielded a ratio of 3:1 in favor of the fast channel.

Additionally, to account for the temporal resolution of the experiment, the calculated time-dependent spectra were convolved with a Gaussian function representing the cross-correlation between the X-ray probe and the UV pump pulses. The FWHM of this Gaussian distribution was treated as an additional free fitting parameter and yielded a value of 145 fs. This value is longer than would be expected from an instrument response function (IRF) associated with the UV-pump and X-ray-probe pulse durations and the time-tool resolution,

which should be approximately 70 fs. This could indicate that there are dissociation processes that show a delayed onset on a timescale comparable to our laser pulse cross-correlation or that the effect of the broad velocity distribution is being accounted for by a lower temporal resolution in the fit.

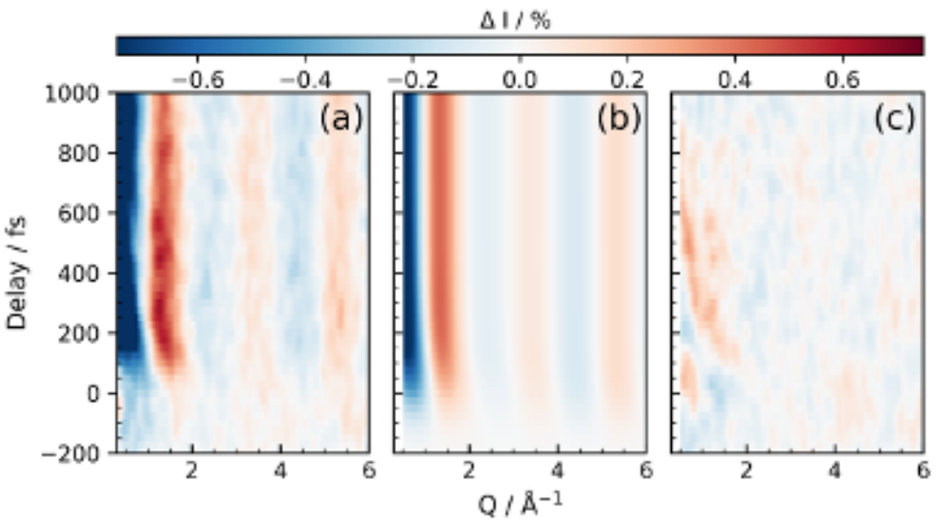

Figure 4: Comparison of time-resolved difference scattering patterns between (a) measured data, (b) fitted data as described in text. Panel (c) showing the residual difference between data and fit.

The resulting best-fit spectrum is shown in Figure 4(b). To aid in visualizing the quality of the fit, the measured scattering pattern shown in Figure 1 is reproduced in Figure 4 panel (a) and the residual difference between measurement and fit is shown in panel (c). A common color scale was used for all three panels. The fit shows qualitative agreement with the experimental data across the full time range, accurately capturing the positions of the main features of the time-resolved scattering signal. However, a considerable residual signal remains at early time delays, indicating that the simple two-channel, constant-velocity distribution model does not fully account for all aspects of the observed dynamics.

A likely source of this discrepancy is the assumption of complete rigidity of the thiophenyl co-fragment. This simplification neglects any structural relaxation of the fragment following photoexcitation. In reality, the photodissociation is initiated from an excited-state

geometry that differs from the final asymptotic geometry, and the co-fragment likely undergoes more significant internal energy redistribution en route to its final structure. Such relaxation dynamics would be most pronounced at early times, consistent with the pattern of residual error observed, and would directly influence the evolving scattering signal in a way that a rigid-body model cannot capture. Accurately modeling this behavior would require incorporation of a time-dependent molecular structure for the co-fragment, guided by trajectory calculations or *ab initio* dynamics simulations. However, in the absence of such calculations for this system, introducing a time-evolving geometry would require speculative assumptions and an impractically large number of free parameters, making the fitting process under-constrained and physically unjustifiable.

To improve the quality of the fit within the constraints of the current model, several modifications were explored. First, a time offset between the onset of the slow and fast dissociation channels was introduced to account for the possibility of a predissociation pathway.[26] Second, a period of initial acceleration was incorporated into the model, allowing for non-constant velocity dissociation dynamics. However, neither modification led to a significant improvement: in both cases, the least-squares fitting algorithm failed to converge to a minimum residual error, suggesting that more fundamental refinements, particularly those addressing time-dependent molecular geometry, are required to capture the full complexity of the observed dynamics.

The persistent residual signal at early time delays, suggests that, apart from translational motion, internal degrees of freedom may also significantly influence the observed scattering dynamics. While a full treatment of the evolving geometry of the dissociating system is not feasible in the absence of high-level excited-state trajectory calculations, insights can still be gained by probing how energy is partitioned between translational, vibrational, and rotational modes following C–I bond cleavage. Such energy redistribution directly affects the observed scattering pattern and may help explain the deviations from the simplified constant-velocity model.

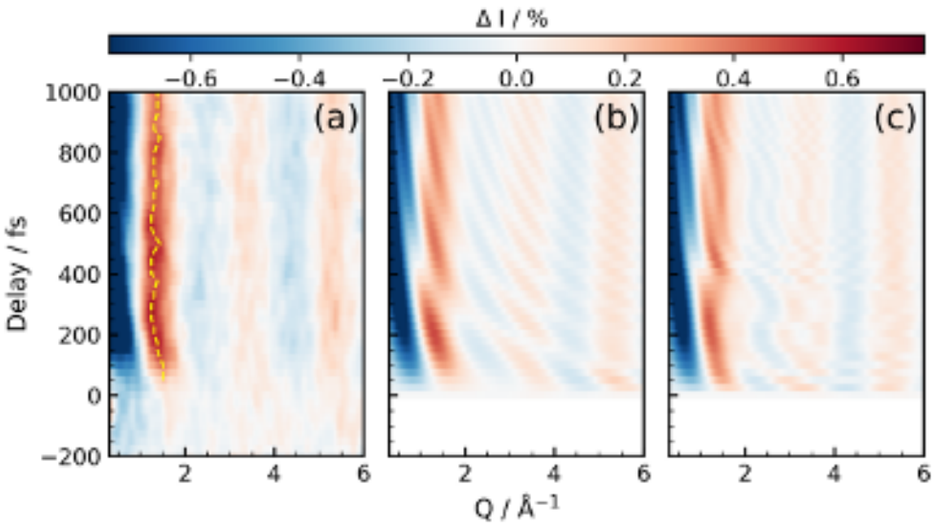

Figure 5: Comparison of time-resolved difference scattering patterns between (a) measured data, (b) data calculated using a simple model at a single interfragment dissociation velocity of 12.0 Å ps^{-1} and (c) data calculated using a simple model at a single interfragment dissociation velocity of 12.0 Å ps^{-1} including rotation of the molecular co-fragment. In panel (a) the dashed yellow line marks the shifting position of maimum intensity as a function of delay.

To this end, we examined the extracted dissociation velocity distributions in the context of energy conservation. The maximum allowed dissociation velocities, $v_{\max}$, are 28 Å ps^{-1} for ground-state I and 19 Å ps^{-1} for spin–orbit excited I* atom products, marked in Figure 2 by black arrows. It should be noted that both dissociation channels are expected to produce a mixture of I and I* atoms, and the scattering experiment does not differentiate between these two electronic states. Consequently, the velocity distributions envelop both products, and the extracted peak positions cannot be uniquely assigned to either I or I* atom products. This interpretation is supported by previous REMPI measurements by Marchetti et al. (see Fig. 2b)), where state-selective detection reveals partially overlapping velocity distributions for I and I* atomic products at an excitation wavelength of 254.7 nm.[23] The experimentally extracted distribution is therefore expected to represent a weighted sum of the I and I* product-channel contributions. We note that the mismatch in relative intensities at low recoil velocities between the distributions derived in the present and earlier studies may

reflect differences in the employed excitation wavelengths.

Nevertheless, the fast dissociation channel peaks close to $v_{\max}$, while the slow channel is centered at significantly lower velocities. This implies that in the second case a significant fraction of the available energy is partitioned into internal degrees of freedom. This is consistent with previous studies.[23,26] To investigate the influence of product rotation, additional simulations were performed incorporating rigid-body rotation of the thiophenyl co-fragment. A single representative interfragment dissociation velocity of 12 Å ps^{-1} was used, approximating the average of the two channels, and 10% of the remaining available energy (after bond cleavage and translational partitioning) was arbitrarily assigned to in-plane rotation of the thiophenyl radical about its center of mass. For simplicity, only ground-state I atom production was assumed, and no predissociation or IRF convolution was included. It is important to note that this model is not intended as a rigorous or quantitatively accurate description of the dynamics. Rather, the purpose is to qualitatively explore how product rotation (within plausible energetic bounds) might alter the shape and features of the scattering signal. The resulting difference scattering pattern was computed using the same methodology described previously.

The results are presented in Figure 5, panel (a) shows the experimental scattering pattern, panel (b) shows the results of the original simple model at a singular interfragment dissociation velocity of 12.0 Å ps^{-1}, and panel (c) shows the data calculated (also at a singular interfragment dissociation velocity of 12.0 Å ps^{-1}) using the simple model with an additional rotation of the co-fragment. Interestingly, restricting the interfragment dissociation velocity distribution to a single representative value reproduces features of the experimental data that were absent in the original multi-velocity model, mainly subtle modulations in the temporal intensity profile. The inclusion of product rotation produced only minor changes, indicating that rotation alone is unlikely to account for the observed discrepancies.

Nonetheless, this analysis offers valuable insight into the interpretation of the Hough transform results discussed earlier. The improved agreement achieved with a single inter-

fragment velocity suggests that the Hough transform may systematically overestimate the width of the dissociation velocity distribution, particularly in systems where product rotation and vibrations are a significant feature of the dynamics. This overestimation can artificially smooth the observed pattern as more geometries are averaged. These findings underscore the importance of exercising caution when interpreting velocity spreads derived from FRXS data via the Hough transform, and highlight the need for complementary modeling approaches that explicitly incorporate rotational and vibrational motions of the products from arising from the dissociation of polyatomic molecules.

Discussion

The photodissociation dynamics of 2IT following 252 nm excitation reveal intricate behavior that can be described by considering the underlying potential energy surfaces and energy partitioning mechanisms. Two primary dissociation pathways were identified in the present work, consistent with previous studies,[23,24,26] offering further evidence of concurrent dissociation pathways.

The increased absorption cross-section at 252 nm suggests that most excitation populates states with substantial $\pi\pi^*$ character in the vertical region.[26] Some of these adiabatic states also have, or acquire, substantial $(n/\pi)\sigma^*$ character on extending the C-I bond and undergo prompt bond cleavage leading to I and I* products. The observed fast dissociation channel yielding products with a relative dissociation velocity of 17.0 Å ps^{-1}, close to the maximum allowed by energy conservation, matches well with previously reported TKER values.[23,26] The steeply repulsive nature of the $(n/\pi)\sigma^*$ surfaces along the C-I bond coordinates facilitates rapid bond extension with minimal barriers, accounting for the products being released with high kinetic energies.

In addition to the fast channel, a slower dissociation pathway was observed, characterized by a velocity of 6.4 Å ps^{-1}. This channel is consistent with excitation into quasi-bound $\pi\pi^*$ levels, which predissocate by non-adiabatic coupling to the dissociative $(n/\pi)\sigma^*$ continua,

as proposed in our previous work.[26] In this case, nuclear motion in the quasi-bound state is required to reach a conical intersection with the dissociative $(n/\pi)\sigma^*$ potentials, resulting in longer dissociation times and slower product recoil velocities. The approximate branching ratio of 3:1 in favor of the fast channel, compared to 23:1 observed at 262 nm,[26] provides further evidence that the two channels result from excitation into superposition of states of different character.

Analysis of the asymptotic scattering pattern provides clear evidence that the thiophenyl ring remained intact after the C–I bond cleavage, with little reason to suspect ring opening or rearrangement on the timescale of the experiment. This result implies that dissociation occurs primarily from states where the thiophenyl framework remains structurally stable without substantial distortion along the ring-opening coordinates.

The simple constant-velocity C–I bond extension model including two velocity distributions and treating the thiophenyl radical as a rigid co-fragment, captures the main features of the measured scattering pattern well; however, significant discrepancies remain in the residuals. Attempts to improve the model by introducing time delays or initial acceleration phases were unsuccessful, indicating that more subtle dynamic effects are involved. Notably, simulations assuming a single representative dissociation velocity better reproduced fringes seen in the experimental diffraction signals (as highlighted by dashed lines in Figure 5) which are completely smoothed out whenincorporating the full velocity distributions extracted via the Hough transform. This suggests that, as was postulated, the Hough transform likely overestimates the actual velocity spread and should be considered an upper bound rather than an absolute measure. Further refinement of the model by incorporating rotational excitation of the thiophenyl radical—allocating 10% of the available energy after bond cleavage to rotation yielded only modest changes to the pattern.

Within the scope of this work the residual error between the data and the fitted model persists at short time delays and may indicate minor alternative pathways. Based on the analysis of the asymptotic spectra these are unlikely to be signatures of a ring opening

pathway but are most likely caused by transient species formed along the way towards the conical intersections between the $\pi\pi^*$ and $(n/\pi)\sigma^*$ states. Further work involving detailed potential energy surface calculations and trajectory-based simulations would be valuable to fully capture the dynamics and resolve these outstanding contributions.

Conclusions

This work demonstrates the power of ultrafast X-ray scattering to simultaneously capture the fate of both fragments during complex molecular photodissociation processes. Following 252 nm excitation of 2-iodothiophene, we have directly observed two competing C-I bond cleavage pathways with markedly different dynamics: a fast channel (17.0 Å ps^{-1}) arising from direct $(n/\pi)\sigma^*$ excitation, and a slower pathway (6.4 Å ps^{-1}) proceeding via initial $\pi\pi^*$ population followed by nonadiabatic coupling to dissociative surfaces. The 3:1 branching ratio favoring the fast channel reflects the wavelength-dependent absorption cross-sections and represents a significant shift from longer wavelength studies, providing quantitative insight into state-specific photochemistry.

Crucially, structural analysis strongly suggests that the thiophenyl ring remains intact following the dissociation, ruling out ring-opening as a primary relaxation pathway at this excitation energy. This finding resolves long-standing questions about the co-fragment's fate and establishes that energy redistribution occurs primarily through vibrational and rotational excitation of the closed-ring thiophenyl radical rather than through structural rearrangement.

The successful application of FRXS analysis, enhanced by Hough transform feature extraction, represents a methodological advance for studying increasingly complex molecular systems where traditional spectroscopic approaches face limitations. While our simplified dynamical models capture the primary dissociation signatures, the persistent residual signals point toward subtle early-time dynamics that warrant future investigation through high-level

trajectory calculations.

While elements of the obtained information could in-principle come from other methods, for example the extraction of asymptotic velocity distributions from translational kinetic energy release studies,[23] the ability to measure asymptotic properties of structure, energy partitioning and structural dynamics is unique to diffraction methods. These results establish a new benchmark for real-time structural interrogation of competing photochemical pathways in heterocyclic systems, with broad implications for understanding energy flow and selectivity in photoinduced processes. The ability to simultaneously track bond breaking velocities, energy partitioning, and structural integrity opens new avenues for designing and controlling photochemical reactivity in complex molecular architectures.

Acknowledgement

This work was supported by the AMOS program in the Chemical Sciences, Geosciences, and Biosciences Division of Basic Energy Sciences at the U.S. Department of Energy. I.G. was supported by an NDSEG fellowship. Use of the Linac Coherent Light Source LCLS), SLAC National Accelerator Laboratory, was supported by the U.S. Department of Energy, Office of Basic Energy Sciences, under Contract No. DE-AC02-76SF00515. This work was also supported by the National Institutes of Health grant, S10 OD025079, via the use of the x-ray detector. W.O.R. acknowledges the STFC XFEL Physical Sciences Hub and the University of Southampton for a Ph.D. studentship as well as funding by an EPSRC Doctoral Prize. R.S.M. acknowledges financial support from the Leverhulme Trust via Grant No. RPG-2021-257. P.M.W. acknowledges funding by the U.S. Department of Energy, Office of Science, Basic Energy Sciences, Award No. DE-SC0017995, and the National Science Foundation (NSF), Award No. CHE-2309434. A.M.G. was supported by an NSF Graduate Research Fellowship. D.A.H. and G.L.A. acknowledge support by The Netherlands Organization for Scientific Research (NWO) under grant numbers STU.019.009,712.018.004 and VI-VIDI-

193.037. A.E.G. was supported by the European Union, through Horizon Europe project 123-CO: 101067645.

References

(1) Gabalski, I.; Ware, M. R.; Bucksbaum, P. H. X-ray scattering signatures of early-time accelerations in iodine dissociation. Journal of Physics B: Atomic, Molecular and Optical Physics **2020**, 53, 244002.

(2) Gabalski, I. et al. Transient vibration and product formation of photoexcited CS_2 measured by time-resolved X-ray scattering. The Journal of Chemical Physics **2022**, 157, 164305.

(3) Ware, M. R.; Glownia, J. M.; Al-Sayyad, N.; O'Neal, J. T.; Bucksbaum, P. H. Characterizing dissociative motion in time-resolved x-ray scattering from gas-phase diatomic molecules. Physical Review A **2019**, 100, 033413, Publisher: American Physical Society.

(4) Minitti, M. P.; Budarz, J. M.; Kirrander, A.; Robinson, J. S.; Glownia, J. M.; Kozina, M.; Lemke, H. T.; Sikorski, M.; Feng, Y.; Nelson, S.; Saita, K.; Stankus, B.; Northey, T.; Hastings, J. B.; Weber, P. M. Imaging Molecular Motion: Femtosecond X-Ray Scattering of an Electrocyclic Chemical Reaction. Physical Review Letters **2015**, 114, 255501, Publisher: American Physical Society.

(5) Yong, H.; Zotev, N.; Stankus, B.; Ruddock, J. M.; Bellshaw, D.; Boutet, S.; Lane, T. J.; Liang, M.; Carbajo, S.; Robinson, J. S.; others Determining orientations of optical transition dipole moments using ultrafast X-ray scattering. The Journal of Physical Chemistry letters **2018**, 9, 6556–6562.

(6) Yong, H.; Ruddock, J. M.; Stankus, B.; Ma, L.; Du, W.; Goff, N.; Chang, Y.; Zotev, N.;

Bellshaw, D.; Boutet, S.; others Scattering off molecules far from equilibrium. The Journal of Chemical Physics **2019**, 151, 084301.

(7) Yong, H.; Xu, X.; Ruddock, J. M.; Stankus, B.; Carrascosa, A. M.; Zotev, N.; Bellshaw, D.; Du, W.; Goff, N.; Chang, Y.; others Ultrafast X-ray scattering offers a structural view of excited-state charge transfer. Proceedings of the National Academy of Sciences **2021**, 118, e2021714118.

(8) Stankus, B.; Yong, H.; Ruddock, J.; Ma, L.; Carrascosa, A. M.; Goff, N.; Boutet, S.; Xu, X.; Zotev, N.; Kirrander, A.; Minitti, M. P.; Weber, P. M. Advances in ultrafast gas-phase x-ray scattering. Journal of Physics B: Atomic, Molecular and Optical Physics **2020**, 53, 234004, Publisher: IOP Publishing.

(9) Stankus, B.; Yong, H.; Zotev, N.; Ruddock, J. M.; Bellshaw, D.; Lane, T. J.; Liang, M.; Boutet, S.; Carbajo, S.; Robinson, J. S.; others Ultrafast X-ray scattering reveals vibrational coherence following Rydberg excitation. Nature Chemistry **2019**, 11, 716–721.

(10) Ma, L.; Goff, N.; Carrascosa, A. M.; Nelson, S.; Liang, M.; Cheng, X.; Yong, H.; Gabalski, I.; Huang, L.; Crane, S. W.; others Quantitative x-ray scattering of free molecules. Journal of Physics B: Atomic, Molecular and Optical Physics **2024**, 57, 205602.

(11) Ma, L.; Du, W.; Yong, H.; Stankus, B.; Ruddock, J. M.; Carrascosa, A. M.; Goff, N.; Chang, Y.; Zotev, N.; Bellshaw, D.; others Revealing the reaction path of UVC bond rupture in cyclic disulfides with ultrafast x-ray scattering. Science Advances **2025**, 11, eadp9175.

(12) Bucksbaum, P. H.; Ware, M. R.; Natan, A.; Cryan, J. P.; Glownia, J. M. Characterizing multiphoton excitation using time-resolved x-ray scattering. Physical Review X **2020**, 10, 011065.

(13) Ware, M. R.; Glownia, J. M.; Natan, A.; Cryan, J. P.; Bucksbaum, P. H. On the limits of observing motion in time-resolved X-ray scattering. Philosophical Transactions of the Royal Society A **2019**, 377, 20170477.

(14) Ruddock, J. M.; Zotev, N.; Stankus, B.; Yong, H.; Bellshaw, D.; Boutet, S.; Lane, T. J.; Liang, M.; Carbajo, S.; Du, W.; others Simplicity beneath complexity: Counting molecular electrons reveals transients and kinetics of photodissociation reactions. Angewandte Chemie **2019**, 131, 6437–6441.

(15) Ware, M. R. From Time-resolved to Frequency-resolved X-ray Scattering. Ph.D. thesis, Stanford University, 2019.

(16) Wu, X.-F.; Zheng, X.; Wang, H.-G.; Zhao, Y.-Y.; Guan, X.; Phillips, D. L.; Chen, X.; Fang, W. A resonance Raman spectroscopic and CASSCF investigation of the Franck–Condon region structural dynamics and conical intersections of thiophene. The Journal of Chemical Physics **2010**, 133, 134507.

(17) Cui, G.; Fang, W. Ab Initio Trajectory Surface-Hopping Study on Ultrafast Deactivation Process of Thiophene. The Journal of Physical Chemistry A **2011**, 115, 11544–11550, PMID: 21928804.

(18) Schnappinger, T.; Kölle, P.; Marazzi, M.; Monari, A.; González, L.; de Vivie-Riedle, R. Ab initio molecular dynamics of thiophene: the interplay of internal conversion and intersystem crossing. Phys. Chem. Chem. Phys. **2017**, 19, 25662–25670.

(19) Prlj, A.; Curchod, B. F. E.; Corminboeuf, C. Excited state dynamics of thiophene and bithiophene: new insights into theoretically challenging systems. Phys. Chem. Chem. Phys. **2015**, 17, 14719–14730.

(20) Pederzoli, M.; Pittner, J. A new approach to molecular dynamics with non-adiabatic and spin-orbit effects with applications to QM/MM simulations of thiophene and selenophene. The Journal of Chemical Physics **2017**, 146, 114101.

(21) Schalk, O.; Larsen, M. A. B.; Skov, A. B.; Liisberg, M. B.; Geng, T.; Sølling, T. I.; Thomas, R. D. Time-Resolved Photoelectron Studies of Thiophene and 2,5-Dimethylthiophene. The Journal of Physical Chemistry A **2018**, 122, 8809–8818, PMID: 30354137.

(22) Pathak, S. et al. Tracking the ultraviolet-induced photochemistry of thiophenone during and after ultrafast ring opening. Nature Chemistry **2020**, 12, 795–800.

(23) Marchetti, B.; Karsili, T. N. V.; Kelly, O.; Kapetanopoulos, P.; Ashfold, M. N. R. Near ultraviolet photochemistry of 2-bromo- and 2-iodothiophene: Revealing photoinduced ring opening in the gas phase? The Journal of Chemical Physics **2015**, 142, 224303.

(24) Toulson, B. W.; Hait, D.; Faccialà, D.; Neumark, D. M.; Leone, S. R.; Head-Gordon, M.; Gessner, O. Probing C–I bond fission in the UV photochemistry of 2-iodothiophene with core-to-valence transient absorption spectroscopy. The Journal of Chemical Physics **2023**, 159, 034304.

(25) Zhu, H.-L.; Liu, J.; Zheng, X.; Phillips, D. L. Resonance Raman study of the A-band short-time photodissociation dynamics of 2-iodothiophene. The Journal of Chemical Physics **2006**, 125, 054510.

(26) Razmus, W. O.; Allum, F.; Harries, J.; Kumagai, Y.; Nagaya, K.; Bhattacharyya, S.; Britton, M.; Brouard, M.; Bucksbaum, P. H.; Cheung, K.; others Exploring the ultrafast and isomer-dependent photodissociation of iodothiophenes via site-selective ionization. Phys. Chem. Chem. Phys. **2024**, 26, 12725–12737.

(27) Boutet, S.; Williams, G. J. The coherent X-ray imaging (CXI) instrument at the Linac Coherent Light Source (LCLS). New Journal of Physics **2010**, 12, 035024.

(28) Mozzanica, A.; Andrä, M.; Barten, R.; Bergamaschi, A.; Chiriotti, S.; Brückner, M.; Dinapoli, R.; Fröjdh, E.; Greiffenberg, D.; Leonarski, F.; others The JUNGFRAU de-

tector for applications at synchrotron light sources and XFELs. Synchrotron Radiation News **2018**, 31, 16–20.

(29) Harmand, M.; Coffee, R.; Bionta, M. R.; Chollet, M.; French, D.; Zhu, D.; Fritz, D.; Lemke, H.; Medvedev, N.; Ziaja, B.; others Achieving few-femtosecond time-sorting at hard X-ray free-electron lasers. Nature Photonics **2013**, 7, 215–218.

(30) Northey, T.; Kirrander, A.; Weber, P. M. Extracting the electronic structure signal from X-ray and electron scattering in the gas phase. J. Synchrotron Radiat. **2024**, 31, 303–311.

(31) Mardirossian, N.; Head-Gordon, M. ωB97X-V: A 10-parameter, range-separated hybrid, generalized gradient approximation density functional with nonlocal correlation, designed by a survival-of-the-fittest strategy. Phys. Chem. Chem. Phys. **2014**, 16, 9904–9924.

(32) Caldeweyher, E.; Ehlert, S.; Hansen, A.; Neugebauer, H.; Spicher, S.; Bannwarth, C.; Grimme, S. A generally applicable atomic-charge dependent London dispersion correction. The Journal of Chemical Physics **2019**, 150, 154122.

(33) Weigend, F.; Ahlrichs, R. Balanced basis sets of split valence, triple zeta valence and quadruple zeta valence quality for H to Rn: Design and assessment of accuracy. Phys. Chem. Chem. Phys. **2005**, 7, 3297–3305.

(34) Neese, F. Software update: The ORCA program system—Version 5.0. Wiley Interdisciplinary Reviews: Computational Molecular Science **2022**, 12, e1606.

(35) Figueira Nunes, J. P. et al. Monitoring the Evolution of Relative Product Populations at Early Times during a Photochemical Reaction. Journal of the American Chemical Society **2024**, 146, 4134–4143, PMID: 38317439.